Title

Effect of Surface Morphology and Temperature on the Structural Stability of Nanoscale Wavy Films

Authors

A. Adnan and C. T. Sun*

School of Aeronautics and Astronautics, Neil Armstrong Hall of Engineering

Purdue University, 701 West Stadium Avenue West Lafayette, Indiana 47907-2023, USA

*Email: sun@purdue.edu

Abstract

The atomic scale structural stability of freestanding wavy gold (Au) nanofilms was investigated using molecular dynamics simulations. The waviness in the Au film was formed by cleaving sinusoidal surfaces from a {100}<100> bulk crystal. The degree of waviness was varied by changing the wavelength of the sinusoidal surface profile. Films were then equilibrated at different temperatures (between 10 K and 1080 K) and their structural stability was monitored. The MD simulation results revealed that the stability of films depends on temperature and as well as the waviness of the film surface. It was shown that the size dependent melting point depression of Au plays the dominant role in causing the structural instability of wavy films.

1. Introduction

In recent years, design and fabrication of patterned nanostructures have become a popular avenue of research because of their potential applications [1-7] in emerging technologies including fuel cells engineering [1], tissue engineering [2], biomedical engineering [3], creation of counterfeit-resistant documents [4], nanolithography in microelectronics [5], optoelectronics [6], nanomachines [7] and many others. The success of these novel applications, however, lies on one crucial factor – the integrity and stability of the patterned structures during their manufacturing as well as during their service life.

Predicting material stability from the macroscopic physical laws often becomes challenging due to the size dependent behavior of nanostructured materials [8,9]. It is often argued that the size dependent properties of nanomaterials are largely controlled by the presence of free surfaces. It is evident that the fraction of free surface with respect to total volume linearly increases with the reciprocal size of material, and the surface related events e.g. "surface effects" and "quantum effects" start to contribute dominantly to the overall material properties when the characteristic size falls below some critical length scale. To be more specific, the "surface effects" phenomena are related to surface energy and surface stress, and the "quantum effects" are associated with quantum confinements of materials. From stability point of view, the "surface effects" are believed to control the thermal and structural stability while the "quantum effects" are responsible for optoelectronic stability of materials.

In principle, surface energy γ is considered as an excess energy term which is supplied to the material when a new surface is created from the bulk. When a surface is created, the atoms at the surface planes experience different bonding environment compared to the interior. As a result, the atomic arrangements near the surface differ significantly from those in the interior, and two distinct states of stress exist across the surface layers and in the remaining bulk crystal. The stress at the surface is formally known as "surface stress σ_{ij}" which must be balanced by the interior bulk stresses to attain equilibrium. Since γ and σ_{ij} are associated with material surfaces, their relative magnitude is directly related to the surface/volume ratio (SVR) of materials. At the nanoscale, the fraction of the SVR, so as γ and σ_{ij}, becomes significant; hence, materials

start to show size dependent behavior. A classical example where "surface effects" control the material behaviors can be identified from an event called melting point depression (MPD).

The phenomenon of MPD implies reduction of melting temperature (T_m) and is observed quite frequently in nanostructured materials [10-18]. It is shown both experimentally [14] and thermodynamically [9] that the MPD is also size dependent where T_m of nanomaterials can drop to as low as 60% from the bulk. It is found that most of the experimental and theoretical observations of MPD [10-18] can be well predicted by a model theorized by Pawlow [8]. While the model was originally developed for spherical particle clusters, it can be easily generalized for any shapes of nanostructured materials with a suitable geometric factor. Such a generalized model follows the form,

$$\frac{T_m(r)}{T_m^{bulk}} = 1 - \left(\frac{1}{r}\right)\frac{B}{H_m^{bulk}\rho_s}\left\{\gamma_s - \gamma_l\left(\frac{\rho_s}{\rho_l}\right)^{2/3}\right\} \quad (1)$$

where $T_m(r)$ is the size-dependent melting point of a material with characteristic size r, T_m^{bulk} is the bulk melting temperature, B is the geometric factor, H_m^{bulk} is the bulk heat of fusion, ρ is the density and γ is the surface energy. Subscripts s and l denote, respectively, solid and liquid state of materials.

Similar to MPD, size dependent excitation energy due to "quantum effects" are also found, both experimentally [18-20] and theoretically [21-24], in nanomaterials for which many nanostructured optoelectronic devices exhibit photoluminescence (PL) frequency shift. Such shifting occurs due to non-linear increase in ground-state excitation energy (E_g) with the reduction of material size as demonstrated by Hanamura [21] as,

$$E_g(R) = E_g^0 - \frac{1}{(m_e^* + m_h^*)}\left(\frac{13.6 m_e^* m_h^*}{m_e \varepsilon_r^2} - \frac{2\pi^2\hbar^2}{R^2}\right) \quad (2)$$

Where E_g (R) is the size dependent band-gap energy, E_g^0 is the corresponding bulk value, ε_r is electricity constant, m_e^* and m_h^* refer to the reduced mass of electron and hole m_e and m_h respectively.

Now, let us consider two materials having the same size "r" but different surface morphology, e.g. roughness. Obviously, the material with a rougher surface would have more surface area than the material with a smoother surface texture. Hence, it can be

argued that the "surface effects" and "quantum effects" of the rough surface would be different from that of the smoother surface, and either the size dependent melting or the optoelectronic behavior of material may not be predicted by Eqn (1) and (2). In other words, the stability of materials, either thermal-structural or optoelectrinic, should be both size and morphology dependent. While there is a vast body of literatures available on the size dependent properties and stability of materials, little is known about the effect of surface morphology on the stability of nanostructured materials.

In this article, we report molecular dynamics (MD) simulation results on the structural stability of freestanding wavy gold (Au) nanofilms. For the sake of simplicity, we did not include any "quantum effect" in our study. It is also worth mentioning that MD simulation is a very powerful tool to obtain thermal-mechanical equilibrium structure of a material system, but its major limitation comes from the fact that it cannot explicitly provide any "quantum effect" on materials behavior. This is another reason why we could not include any "quantum effect" in our study.

In our study, we first developed different wavy Au films by varying the wavelength of a sinusoidal surface profile. We then obtained the equilibrium structure of these films at different temperatures. All these temperatures were chosen sufficiently below the melting temperature of bulk Au. From the MD results, we have shown that the stability of films is both temperature and morphology dependent, and the geometry-induced melting point depression of Au plays the dominant role in structural stability of wavy films.

2. Molecular Dynamics Simulations

2.1 Molecular Models

Molecular models of freestanding wavy thin films were developed by cleaving single crystal bulk gold (Au) with two free surfaces profiled by a sinusoidal function,

$$w = A_0 \sin(2\pi \frac{x}{\lambda}) \tag{3}$$

in which A_0 and λ are, respectively, the amplitude and the wave length of the harmonic surface as shown in Fig. 1. The directions along the x, y and z correspond to the length, width, and thickness of the film, respectively. It can be noted that the films were created from a bulk {100}<100> Au crystal. The dashed box in Fig. 1 represents one of the unit

cells that was simulated by MD. The finite thickness of the unit cell was maintained by applying periodic boundary conditions along x and y directions only.

In this study, the dimensions of the unit cells were chosen to be $40a_0$ in length, $15a_0$ in width, and $15a_0$ in thickness direction. Here a_0 refers to the equilibrium lattice constant of single crystal Au (4.08 Å at 0 K). The variation in surface morphology was modeled by changing the wavelength λ while keeping the amplitude A_0 ($4a_0$) fixed. We chose four different types of wavelengths, namely λ = $40a_0$, $20a_0$,$10a_0$ and $6a_0$. The thickness (~6 nm) of the film was chosen such that it was thick enough to eliminate any "spurious" interactions between the opposite free surfaces. The stability of thin films was studied at five different temperatures, namely at T = 10 K, 270 K, 540 K, 810 K and 1080 K. It is noted that the chosen temperatures are below the melting point of bulk Au (~1337 K) [25,26].

2.2 Force Field

In this work, we have employed the modified Finnis-Sinclair (FS) [27] many-body potential to describe the interatomic interactions of Au films. The modified potential was first implemented by Sutton-Chen [28] and follows the form,

$$U_{SC} = \varepsilon \left[\sum_{i<j} \left(\frac{a_0}{r_{ij}} \right)^n - C \sum_i \rho_i^{1/2} \right] \tag{4}$$

where the local density ρ_i is given by

$$\rho_i = \sum_j \left(\frac{a_0}{r_{ij}} \right)^m \tag{5}$$

in which r_{ij} is the separation between atoms i and j , C is a positive dimensionless parameter, ε is the depth of energy-well, a_0 is equilibrium lattice constant at 0 K, and m and n are positive integers. The local density term in Eqn. (5) introduces the many body effect in the potential and makes the force field more accurate than pair types. The atomic cohesive energy (E_c) and lattice parameters (a_0) were fitted exactly in this potential, which has significant importance in evaluating temperature dependent behavior of materials. The set of parameters for Au and the evaluated mechanical properties [28] are listed in Table 1[†].

Table 1: Potential Parameters for f.c.c Au [21].

m	n	ε (ev)	C	Lattice Constant a_0 (Å)	Cohesive Energy, E_c (ev/atom)
8	10	1.2793×10^{-2}	34.408	4.08	3.78

2.3 Simulation Procedure

The MD simulations for various nanocrystalline Au thin films were conducted at a constant temperature under zero external pressure. From statistical thermodynamics, this method is referred to as isobaric-isothermal ensemble (NPT) simulation [29], and it is numerically performed by including appropriate barostat and thermostat functionals [30] in the original equation of motion. Out of several numerical methods, we have employed the Nosé-Hoover prescribed method [31] in our simulations. Specifically, the temperature and pressure were controlled by thermostats (heat bath) and barostats (pressure bath) respectively, and the time constant for either "bath" was set at 1 ps. The equations of motions were integrated using *Verlet-Leapfrog* algorithm [30] with a 0.5 fs time step.

For a prescribed temperature, the equilibrium structures of bulk Au were obtained from a MD run of 50 ps. In the next step, wavy thin films were created from the relaxed bulk crystals, and then they were equilibrated for at least 100 ps. During this equilibration process, the variation in internal energy with time was monitored, and simulation was terminated when the energy of a film became stabilized with small-scale fluctuations. Such fluctuation in energy is attributed to the thermal vibration of atoms.

3. Results and Discussions

3.1 Stability of Thin Films

Figure 2 displays the MD snapshots of the equilibrated (after 100 ps or later) shapes of the initial freestanding wavy films at five different temperatures. As mentioned earlier, the waviness in the films is defined by Eqn. (3) with the degree of waviness characterized by wavelength λ. It appears from Fig. 2 that at relatively low temperatures ($T \leq 540$ K), wavy films maintained their initial structures fairly well with some local reconstructions of surface atoms. Such reconstructions become more pronounced for surfaces with

shorter wavelengths. Essentially, the reconstructions of the surface atoms take place because of the energy minimization condition, as can be observed from the energy plot in Fig. 3. Figure 3 also confirms that, at T ≤ 540 K, all structures attain their respective minimum energy configurations after an equilibration of 100 ps. In other words, at these temperatures the wavy films remain stable regardless their degrees of waviness. At 810 K, however, the condition for stability appears to become wavelength (λ) dependent. As shown in Fig. 2, Au films maintain their wavy shapes as long as $\lambda > 10a_0$. It appears that films with $\lambda < 10a_0$ no longer can remain wavy and tend to transform towards a flat surface. The energy plots shown in Fig. 3 also suggest that films would experience significant structural changes when λ becomes less than $10a_0$. At 1080 K, all wavy films become unstable and reconfigure themselves to nearly flat surfaces. We observed that the "flattening" process of the film, both at 810K and at 1080K, did not occur suddenly, rather it occurred in a progressive fashion. During this process, the atoms from the "peaks" of the rough films were continuously seen to diffuse towards the "valleys" until the film transformed to a flat surface.

While the energy plots in Fig. 3 show that the resulting shapes are associated with the minimum energy levels, two factors remained unclear – first, whether the extensive reconstruction at the surface affects the interior part of the film, and second, what is the underlying driving force for the stability of wavy film. In order to see what happens to the atoms located in the interior part of the film during the surface reconstruction process, we carefully monitored the entire atomic trajectories during the equilibration process. We, however, did not found any notable changes in the atomic configurations of the interior atoms regardless the degree of reconstructions at the surface. In other words, the surface reconstruction process remained fairly dominant around the surface layers and smeared out quickly towards the interior layers. In the following sections, we attempt to show that the size dependent melting of gold film might have played the controlling role in the geometry- induced stability.

3.2 Size Dependent Melting of Gold Film

It has been mentioned earlier that the melting point of crystalline materials, a unique physical behavior of bulk crystalline solids, becomes size dependent when the

dimensions of the material reduce to nanoscale [9-18]. It is observed that melting point of nanowires [12], nanoparticles [10,11,13-16], or nanocrystalline films [17,18] may be reduced by 50-60% from the bulk. It is, however, difficult to know the exact amount of reduction for a particular material because melting is influenced by many other factors including surface energy and density of materials. While there are a vast body of literatures available on MPD of nanostructures, we did not find any literature that showed the thickness-dependent melting of Au films. We therefore resort to the molecular dynamics method to obtain their melting behavior.

In order to address the size dependent behavior of thin Au film, we simulated a set of atomically flat films and evaluated their melting temperatures. In this part of the study, we chose to model flat films instead of the wavy films to separate out the geometry-induced contribution from the size (thickness) dependent behavior of films. As before, the periodic boundary conditions were applied along the length and width (along x and y-axes) directions only. The dimensions of the simulation box were $30a_0 \times 30a_0$ in the length and width directions, and between $1a_0$ to $10a_0$ in the thickness direction to account for the size effect. The MD simulation was performed with the NPT ensemble at a heating rate of 10 K/ps from T = 10 K to T = 1500 K. The time step employed in the simulation was 1 fs. In Fig. 4(a), the variation of potential energy as a function of temperature is shown, and several observations can be made from the plots as discussed below.

3.2.1 Progressive Melting of thin films

Thermodynamically, the melting of bulk crystalline solids is characterized by a sudden increase in the free energy. This additional energy is supplied from the latent heat of fusion of that particular solid. Accordingly, a single crystal bulk Au melts at 1336 ± 1 K [19,20]. However, it appears from Fig. 4(a) that there exists neither a unique melting temperature nor a size-independent value on the melting of thin films. It is also evident that except for t = 0.408 nm, all films exhibit a general trend in the energy-temperature relation during the heating process. Figure 5 shows one such heating curve corresponding to 3.264 nm thick Au film. It can be seen from Fig. 5 that as the heating process continues, energy first increases almost linearly up to 620 K, and then becomes non-

linear (point A) until a sudden change in slope occurs (point B) at 1000 K after which energy again increases linearly with temperature. We may consider point A and B as the initiation and completion of melting, respectively. Based on this, the size dependent melting (complete) temperature of Au film is reported in Fig. 4(b). In this plot, we did not include the value for 0.408 nm thick film. It can be observed from Fig. 4(a) that energy suddenly drops at ~230 K, and then increases monotonically with a slight change in slope at ~700 K. The sudden drop in energy at 230 K is attributed to the "structural failure" of the film when the original planner structure became unstable, lost structural integrity and transformed to clusters of atoms (not shown here). This suggests that a film with only two atomic layers is not energetically favored. It is noted that defining a melting initiation point is somewhat arbitrary here in the sense that the non-linearity in the energy curve in these temperature ranges is caused by both surface reconstructions and breakage of long-range order (LRO) in the crystal structures. Nevertheless, it is evident that the Au films simulated here do not exhibit a sharp melting point; rather, their melting is progressive in nature.

The reason why these thin films do not exhibit an instantaneous melting point can be explained from the surface energy point of view. It is known that the driving force for the solid to liquid phase change is the latent heat of fusion which must be supplied by some external sources, e.g. heating. Specifically, melting of a solid occurs at some specific energy level that equals the solid-state internal energy plus the latent heat of fusion. As temperature increases, internal energy also increases due to thermal expansion. Because atoms at the surface always remain at higher energy states (by surface tension), they attain the required melting energy at some lower temperature T_i ($T_i < T_m$). The T_i may be considered as the initiation of melting. To capture what happens between melting initiation and completion, we have employed a new phenomenological model as discussed below.

3.2.2 Disorder Index Parameter

It is well known that motions of atoms are always a function of temperature, and there exist a significant difference between the solid and liquid state atomic motions. In principle, crystalline solids must retain their long-range orders (LRO); hence, the solid-state atomic motions are governed by thermal vibrations only. As soon as materials

liquefy, their LRO are destroyed and atoms move more "freely". Such degree of differences in atomic motions in the solid and liquid states is quantitatively related to the melting of materials, and many researchers have attempted to utilize these relations to identify melting of materials [11]. Comparing the temperature dependent diffusion coefficient (D) [34] or Lindemann Index (LI) [32] is two such methods that have been extensively used in the literatures. From MD point of view, measuring local (section by section along a length) diffusion constant D(r) for a material model that is simulated in constant temperature ensemble (NVT, NPT or NσT) is ambiguous because temperature (so as velocity) of each atom is forcefully maintained constant. The calculation of LI [32] requires time-averaged root mean squared (r.m.s) bond length fluctuation. In our view, the estimation of local LI may appear difficult across the interface of melted surface boundary layer and solid interior because defining a bond-length in this region would be somewhat ambiguous. In this situation, it would be more convenient to find a relation between spatial changes of individual atomic positions and their melting behavior. In this study, we propose a new approach that can be effectively utilized for both local and global melting behavior of materials.

In this method, we introduce a parameter named Disorder Index (DI) which is expressed as

$$DI = \frac{1}{2\langle A_0 \rangle N_s} \sum_i |r_i - r_{0i}| \qquad (6)$$

where N_s is the number of atoms present in a sub-volume, $\langle A_0 \rangle$ is the amplitude of thermal oscillations, r_i is spatial position of the i^{th} atom and r_{0i} is the reference position of the same i^{th} atom. In Eqn. 6, the factor 2 appearing in front of A_0 takes into account the maximum separation between two neighboring atoms by thermal motion. It is instructive to note that the reference position r_{0i} should be obtained from an initial unreconstructed configuration. Since N_s can be any number between zero and total atoms N, this method can be applied for any sub-volume whose local behavior is sought. As discussed earlier, atoms experience significant mobility in the liquid phase, but maintain LRO in the solid phase in which the maximum motion is attributed to the amplitude of thermal vibration. As a result, DI attains significantly higher value in the liquid state, but remains close to

unity in the solid state. We show in the subsequent sections that the DI parameters can be readily employed to identify the progressive melting process of thin films.

Figure 6 shows the DI plot of 3.264 nm thick film at four different temperatures. These temperatures are marked in Fig. 5. It is evident from Fig. 5 that T_1 lies in the solid phase, T_2 and T_3 lie in the solid-liquid transition phase and T_4 stays in the liquid phase. It can be observed from Fig. 6 that at low temperatures ($T \sim T_1$) atoms experience uniform thermal oscillations and their DI numbers remain near unity. A slight increase in DI number is found close to the free surfaces obviously reflecting the increased mobility of surface atoms. It is seen that the DI numbers of atoms near the two free surfaces increase considerably at T_2, indicating that the film has melted locally. As the temperature continuously increases, melting takes place in the entire film and liquefaction occurs. The variation in the temperature dependent DI number clearly describe how melting occurs in thin films and why they exhibit progressive melting at the nanoscale.

By comparing the heating curve in Fig. 5 and the DI plots in Fig. 6, it is apparent that the DI can be an accurate tool to quantitatively assess the state of the local phase (liquid or solid) of materials. To understand the stability of thin films, we carefully observed the heating curve of thin film and the corresponding DI parameter as a function of temperature. Of particular interests were 810 K and 1080 K where we observed instability in some (at 810K) or all (1080K) of the initial wavy films. In Fig 7, we have plotted the DI against film thickness at 810 K. It is evident that for all films, some degree of melting occurs in the free surfaces. For thicker films, the depth of these local melting zones is ~$1.5a_0$. Accordingly, films thinner than $3a_0$ are unable to remain solid at 810 K. This is also evident from Fig. 4(b) that films thinner than 1.2 nm (corresponds to $3a_0$) would melt at 810K.

3.3 *Driving Force for thin film instability*

The thin films we have studied here have thickness of $15a_0$ (~6 nm), hence they are thermally stable at 810 K. However, as illustrated in Fig. 8, their local structures at the wavy free surfaces can be contrasted with thin films. It can be visualized from Fig. 8(a) that each of the half sinusoid (outlined by dotted oval) may be considered as a triangle-like thin films (we refer them as sub-films) whose thicknesses linearly vary from

the peak to the valley of the wave. Figure 8(b) shows the relative thickness of the sub-films measured from their corresponding wave peaks. It appears from Fig. 8(b) that depending on the wavelength λ, a significant fraction of the sub-films may appear very thin, and therefore becomes thermally unstable. If we consider the thickness of $3a_0$ as the critical film thickness (t_c) for the melting of Au at 810 K, Fig. 8(b) clearly demonstrates that about 80% of the sub-film remains below the critical thickness level for smaller wavelengths ($\lambda \leq 10a_0$). Accordingly, these sub-films fail to remain stable at 810 K, and then flattened out. It appears from the trends displayed in Fig. 4(b) that the melting temperature of thicker Au films approach ~1050 K implying that all wavy films we studied melt at 1080 K. This explains why wavy surfaces becomes flat at this temperature.

4. Summary and Conclusions

In this study, molecular dynamics simulations of various wavy gold films were performed at different temperatures. The sinusoidal surfaces of the films were formed by cleaving them from a bulk gold in equilibrium. The degree of waviness was controlled by varying the wavelength of the sinusoidal surface. Four different films were thus constructed. The thickness of these films was 6.1 nm. The stability of these thin films was studied at five different temperatures which were below the melting point of bulk gold. It was observed from the equilibrated shapes of these structures that the stability of wavy surfaces significantly depends on temperature and degree of waviness. It was also found that the size dependent melting of Au films occurred in a progressive manner over a range of temperature rather than occurring at some fixed temperature. A new method was to identify the melting temperature of crystal structures, and was employed to display that the progressive melting is caused by the non-uniform melting of film along the thickness direction. The melting in the film starts when only the atomic layers at the two free surfaces melt at temperatures lower than the so-called bulk melting temperature. As heating continues, the entire film then gradually melts.

It is discussed that the low temperature pre-melting of the surface boundary layers plays the foremost role in the instability of wavy films. It is shown than for a particular temperature, e.g. at 810 K, there exist a critical film thickness below which melting occurs in the entire structures; otherwise it is confined at the boundary layers only. It is

recognized that the film thickness of the wavy films were five times thicker than the critical thickness at 810 K. However, it was demonstrated that the surface waviness in the films behaved as secondary thin films, and for smaller wavelengths, the major fractions of the sub-film thickness fell below the critical thickness at 810K. As a result, some wavy films became unstable. At elevated temperatures, e.g. 1080 K or higher, films are unable to maintain their structure due to melting point depression of Au films.

Acknowledgment

The authors gratefully acknowledge support by the National Science Foundation under grant number HRD-976871. We gratefully thank Dr. W. Smith and the Daresbury Laboratory for providing the Molecular Dynamics Simulation Package DL-POLY(2.17) [33].

References

[1] Debe M K, Schmoeckel A K, Vernstrom G D, Atanasoski R 2006 *J. Power Sources*, **161** 1002-1011.

[2] Gadegaard N, Martines E, Riehle MO, Seunarine K and Wilkinson C DW 2006 **83** 1577-1581.

[3] Webster T J, Smith T A 2005 *J. Biom Mats Res* **74A** 77-686.

[4] Phillips G K 2004 *United States Patent* # 6692030.

[5] Bucknall D G (editor) *Nanolithography and patterning techniques in microelectronics* 2005 **(**USA, CRC Press).

[6] Razeghi M, Brown G J 2006 *Proc. of SPIE* **6127** 61270H doi: 10.1117/12.643137

[7] Drexler K E 1999 *Trends in Biotechnology* **17(1)** 5-7.

[8] Fischer F D, Waitz T, Vollath D, Simha N K, 2007 *Prog Mat Sci* doi:10.1016/j.pmatsci.2007.09.001.

[9] Pawlow P 1908 *Z physik Chemie* **65** 1–35.

[10] Lee Y J, Lee E K, Kim S, Nieminen R M 2001 *Phys Rev Lett* **86** 999-1008.

[11] Alavi S, Thompson D L 2006 *J. Phys Chem* A **110** 1518-1523.

[12] Moon W H, Kim H J, Choi C H 2007 *Scrip Ma* **56** 345-348.

[13] Olsen E A, Efremov M Yu., Zhang M, Zhang Z, Allen L H 2005 *J. Appl. Phys* **97** 034304.

[14] Buffat Ph, Borel J-P 1976 *Phys Revs E* **13(6)** 2287-2298.

[15] Shim J-H, Lee B-J, Cho Y W 2002 *Surf Sci* **512**, 262-268.

[16] Coombes, C J 1972 *J. Phys* **2** 441-448.

[17] Gladkikh N T, Bogatyrenkob S I., Kryshtala A P, Anton R 2003 *Appl Sur Sci* **219** 338–346.

[18] Mei Q S, Lu K 2007 *Prog Mat Sci* **52** 1175-1262.

[19] Wu H Z, Qiu D J, Cai Y J, Xu X L, Chen N B 2002 *J Cryst Grow* **245** *50 -55*

[20] Fu Z D, Cui Y S, Zhang S Y, Chen J, Yu D P, Zhang S L, Niu L, Jiang J Z 2007 *Appl Phys Lets* **90** *263113*

[21] Hanamura E 1988 *Phys Rev B* **37(3)** *1273-79*

[22] Efros A L and Efros A L, 1982 *Sov Phys Semicond* **16** *772-5*

[23] Brus J E 1984 *J Lumin* **31** *381-4*

[24] Kayanuma Y 1988 *Phys RevB* **38** *9797-805.*

[25] Sambles J R 1971 *Pro Royal Soc A* **324** 339-351.

[26] Holborn L, Day A L 1901 *Ann Phys* **4** 99-103

[27] Finnis M W, Sinclair J E 1984 *Phil Mag A* **50** 45-56.

[28] Sutton A P, Chen J 1990 *Phil Mag Lett* **61** 139-146.

[29] Hill T L 1986 *An Introduction to Statistical Thermodynamics* (Dover, N. Y., USA).

[30] Allen M P, Tildesley DJ 1987 *Computer Simulations of Liquids* (N. Y., Oxford University Press, USA).

[31] Hoover H G 1985 *Phys Rev A* **A31** 1695-1711.

[32] Lee Y J, Maeng Y, Lee E-K, Kim B, Kim S, Han K-K 2000 *J Comp Chem* **21(5)** 380-387.

[33] Smith W, Forester T R 1996 *J. Mol Grap* **14** 136–41.

[34] Glicksman M E 2000 *Diffusion in Solids: Field Theory, Solid-State Principles, and Applications (*Wiley, NY USA).

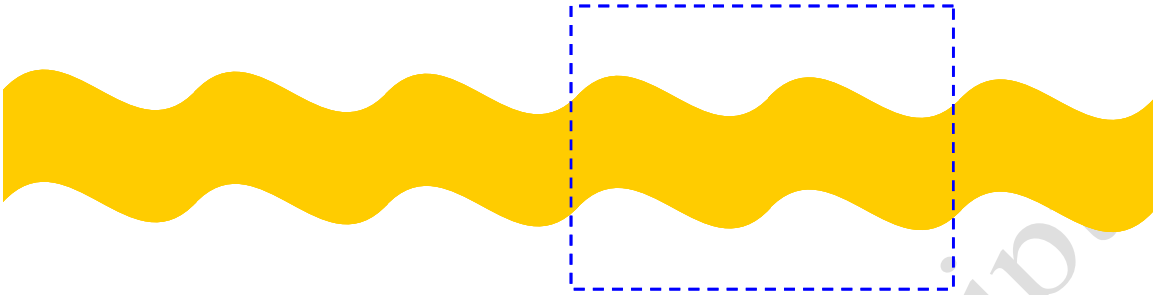

(a)

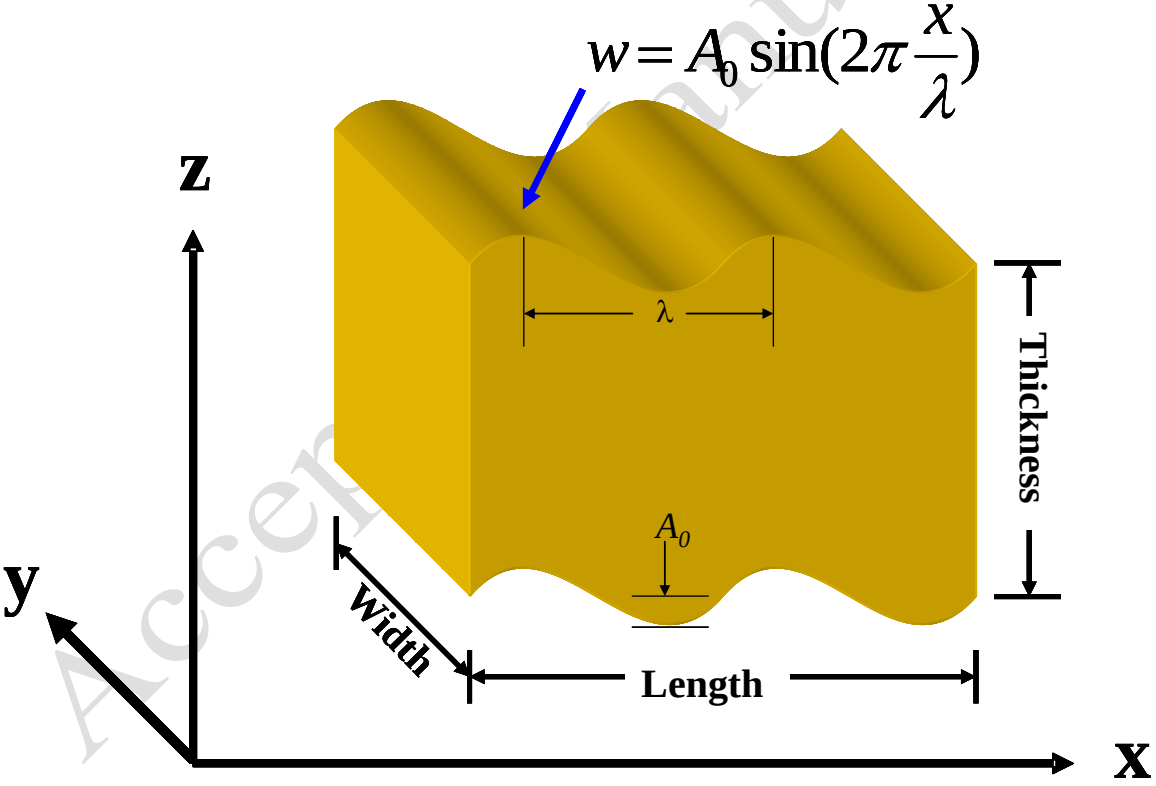

(b)

Figure 1: (a) Schematics of a freestanding wavy film and (b) simulated unit cell in MD.

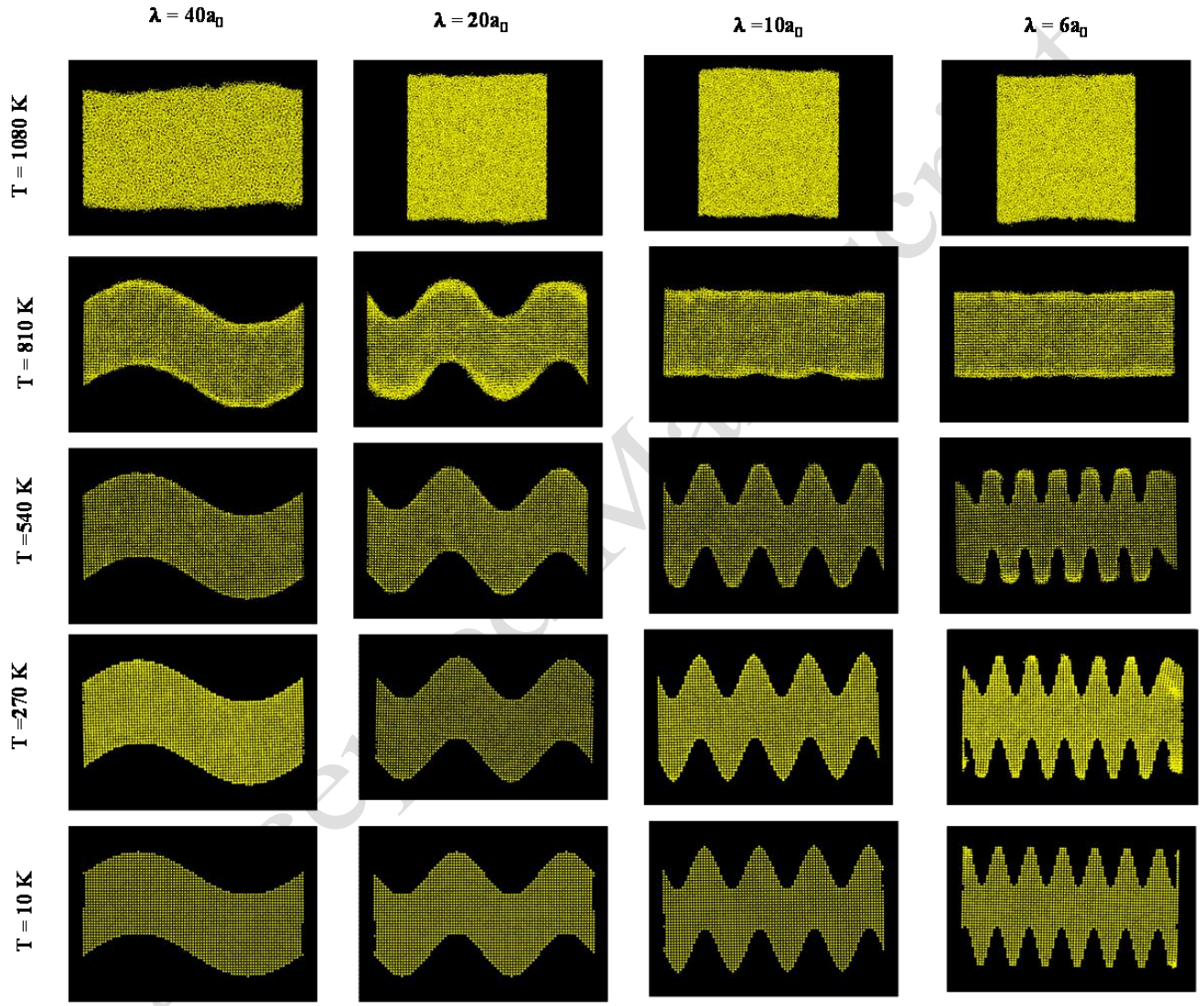

Figure 2: MD snapshots showing equilibrated structures of initially wavy films.

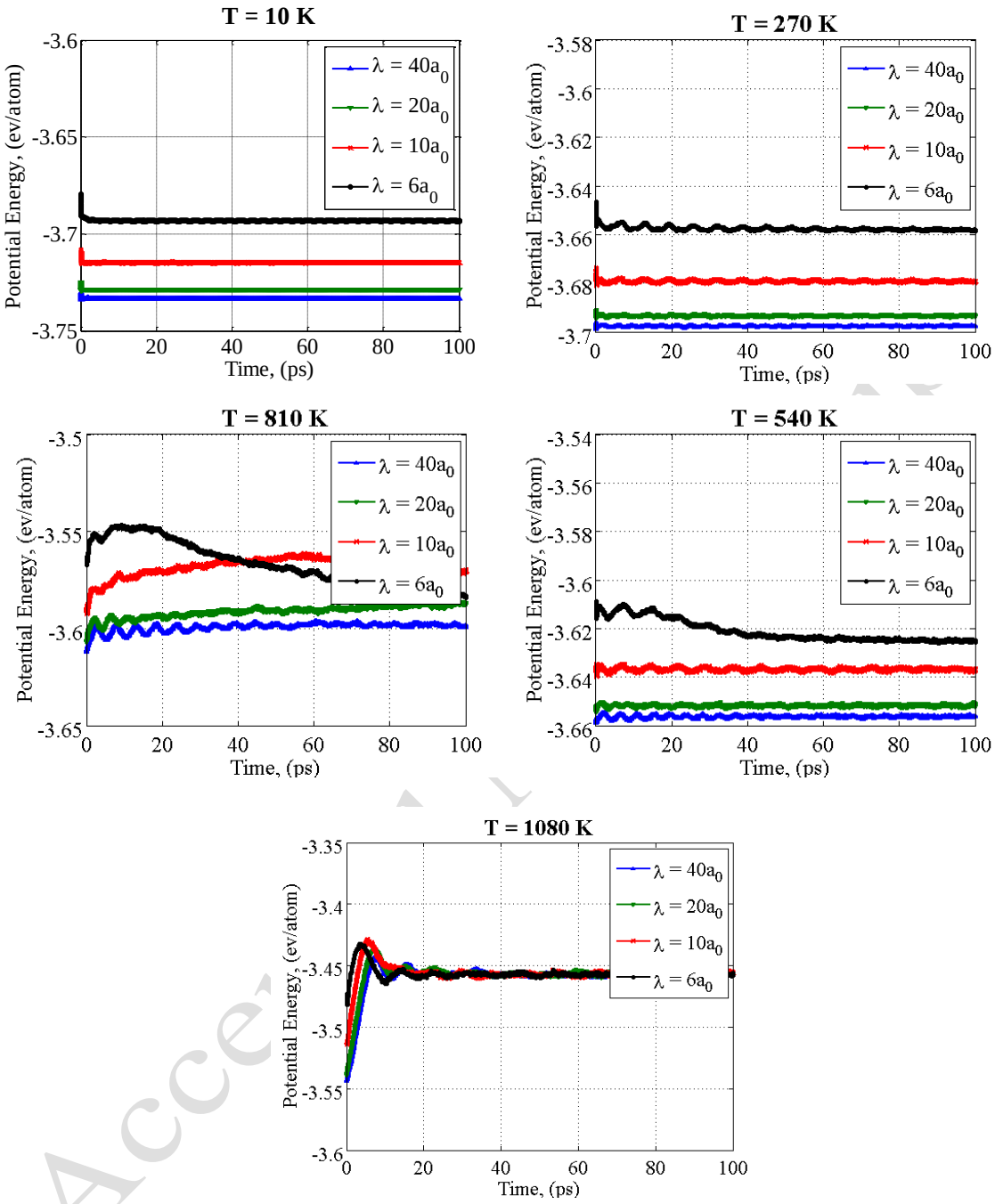

Figure 3: Energy history of wavy films at different temperatures.

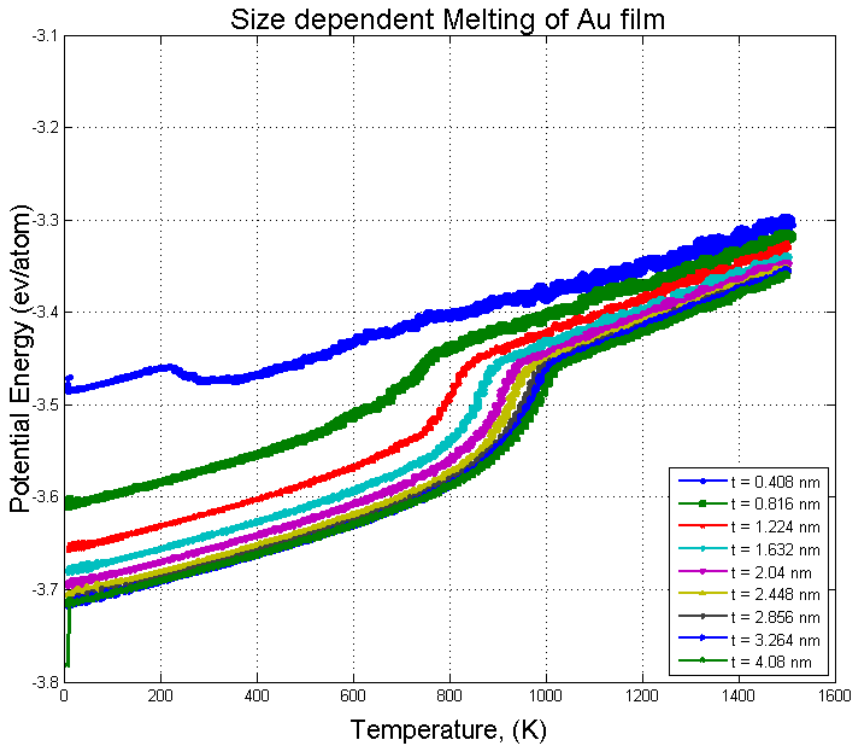

(a)

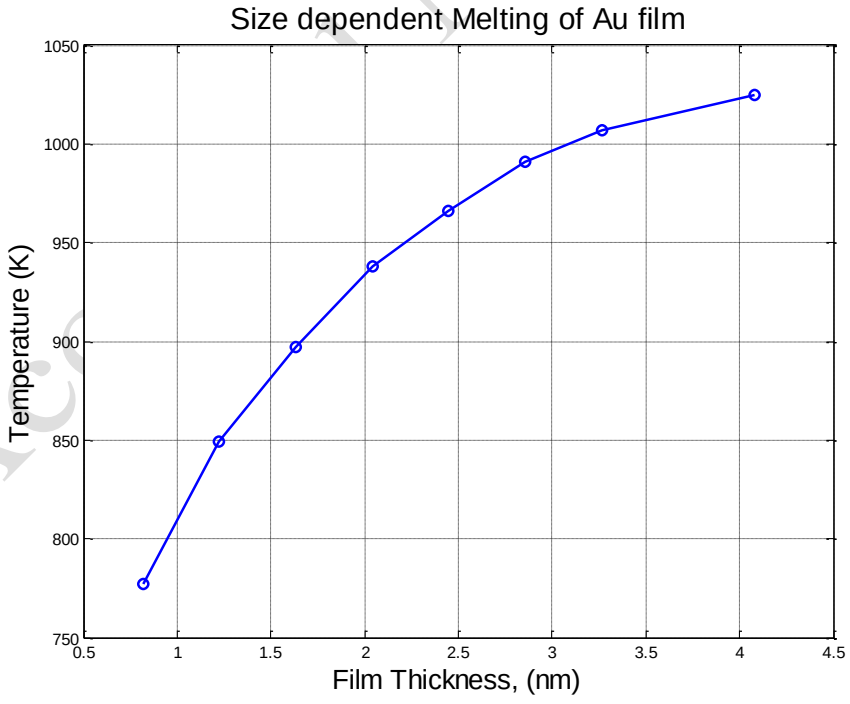

(b)

Figure 4: Thickness dependent melting of free standing Au film: (a) energy vs. temperature plot (b) melting point vs. film thickness curve.

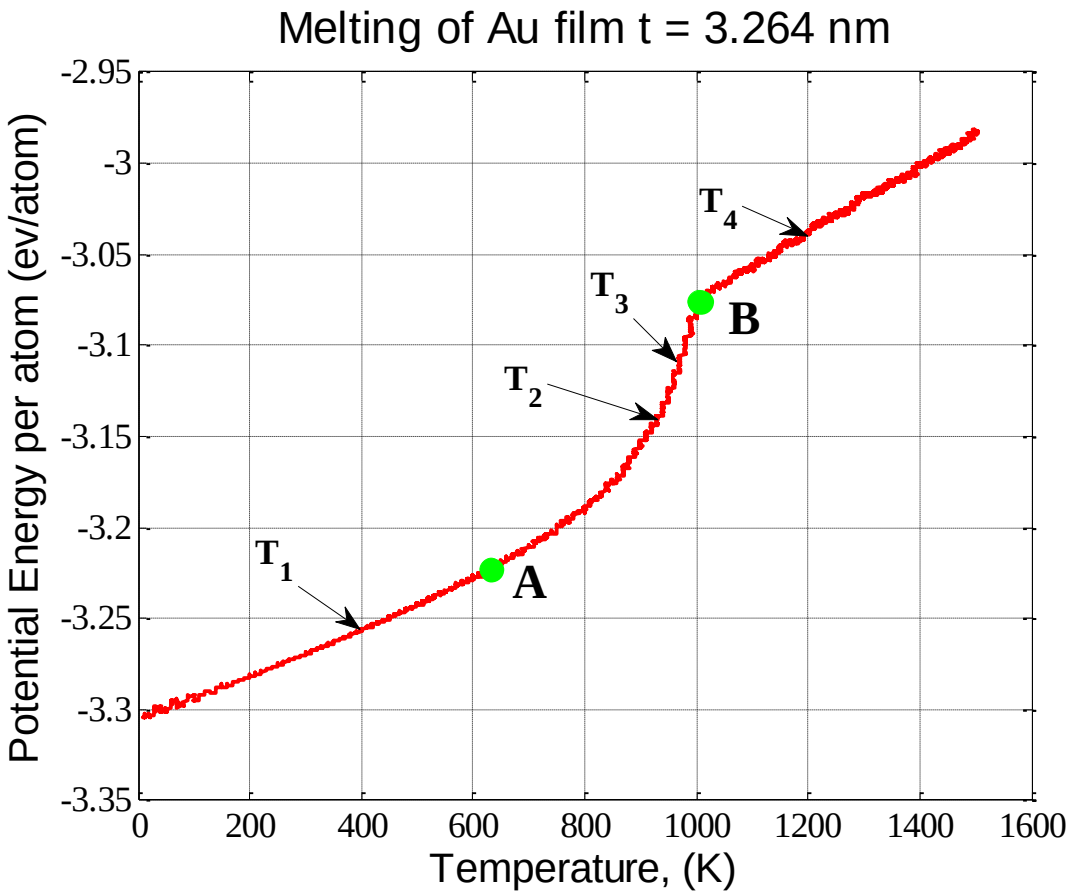

Figure 5: Heating Curve of a 3.264 nm thick Au film showing variation of energy with temperature.

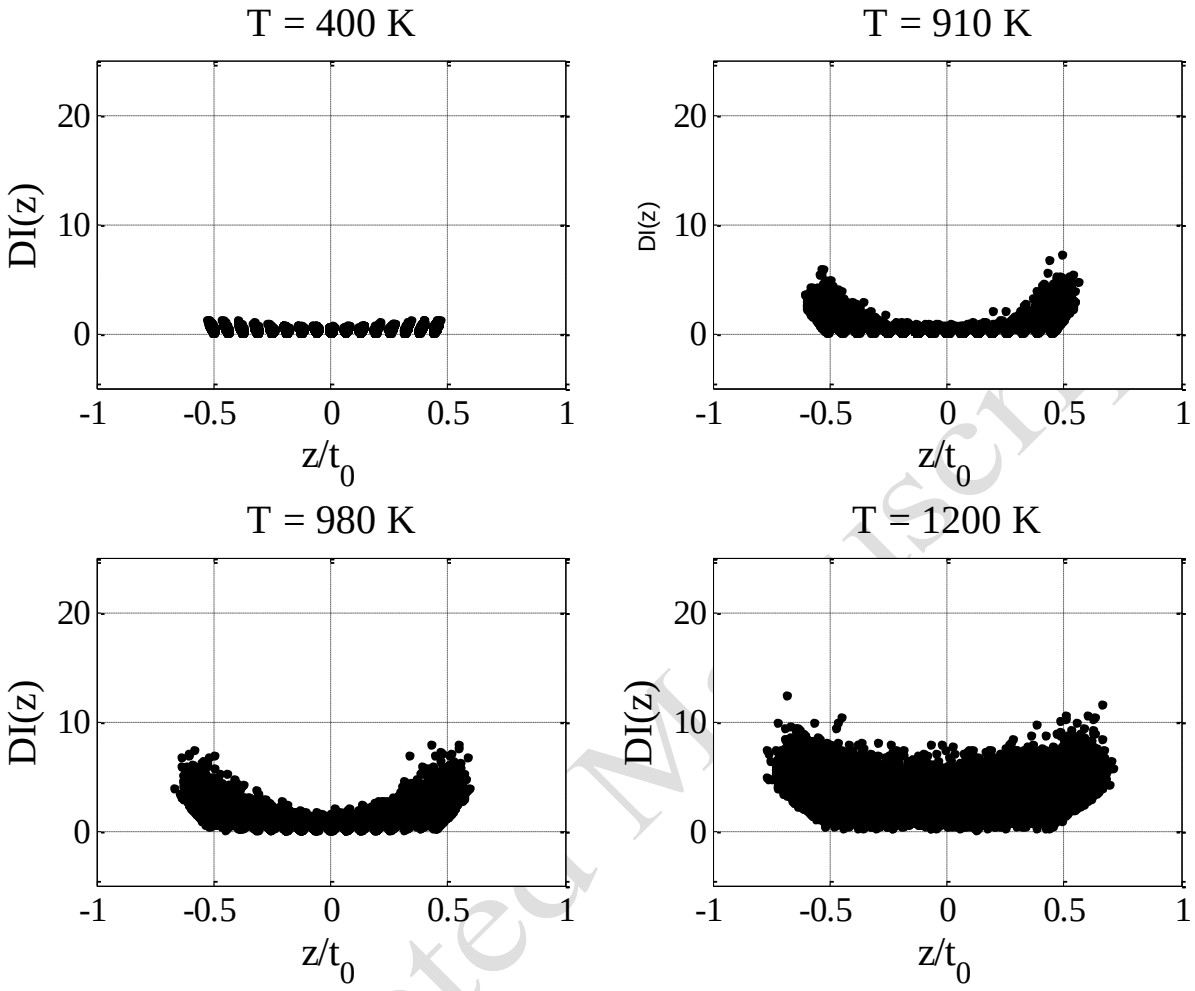

Figure 6: Change in DI parameter with temperature of a 3.264 nm thick Au film.

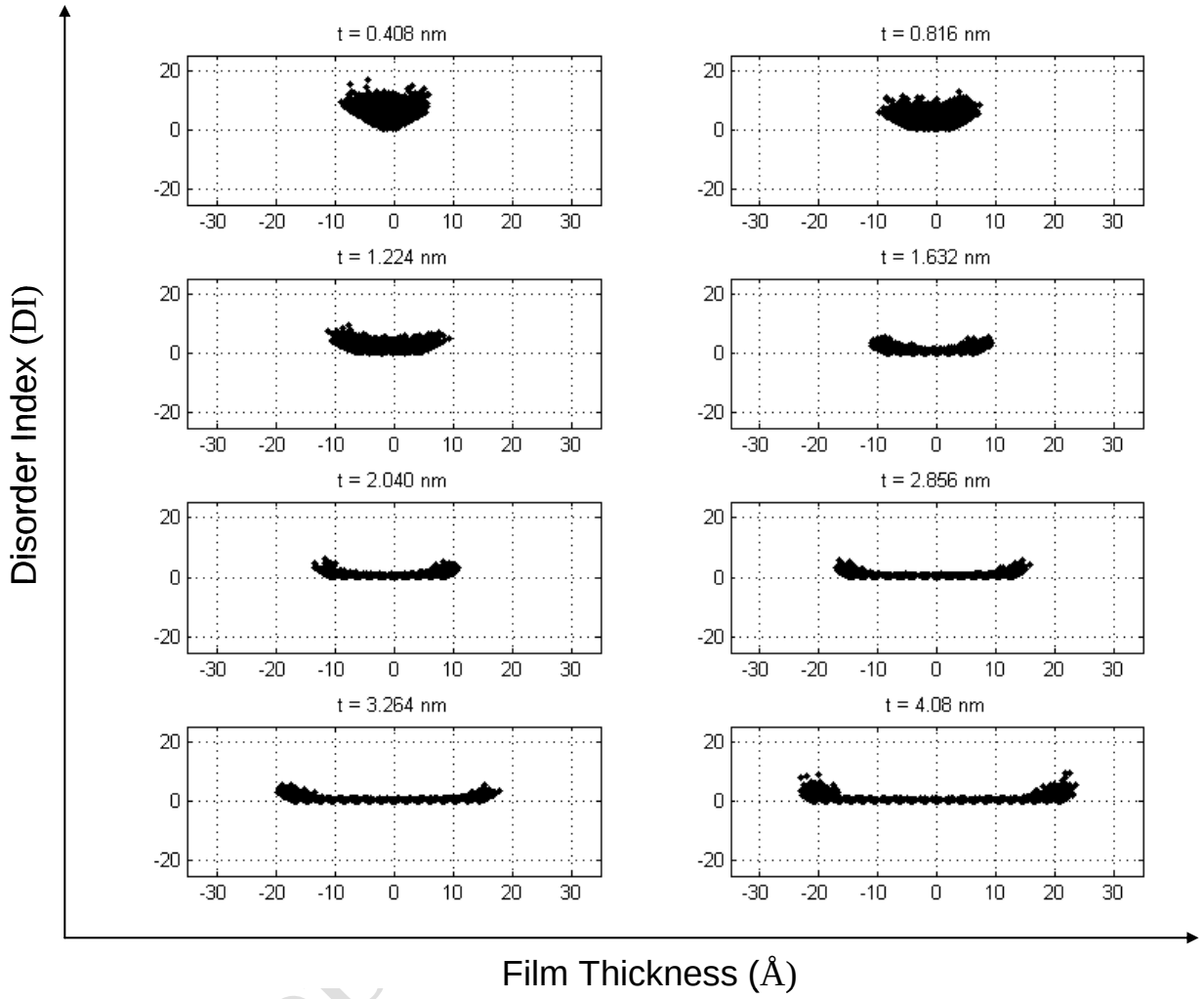

Figure 7: Thickness dependent distribution of DI parameter along the thickness direction of Au film at 810 K.

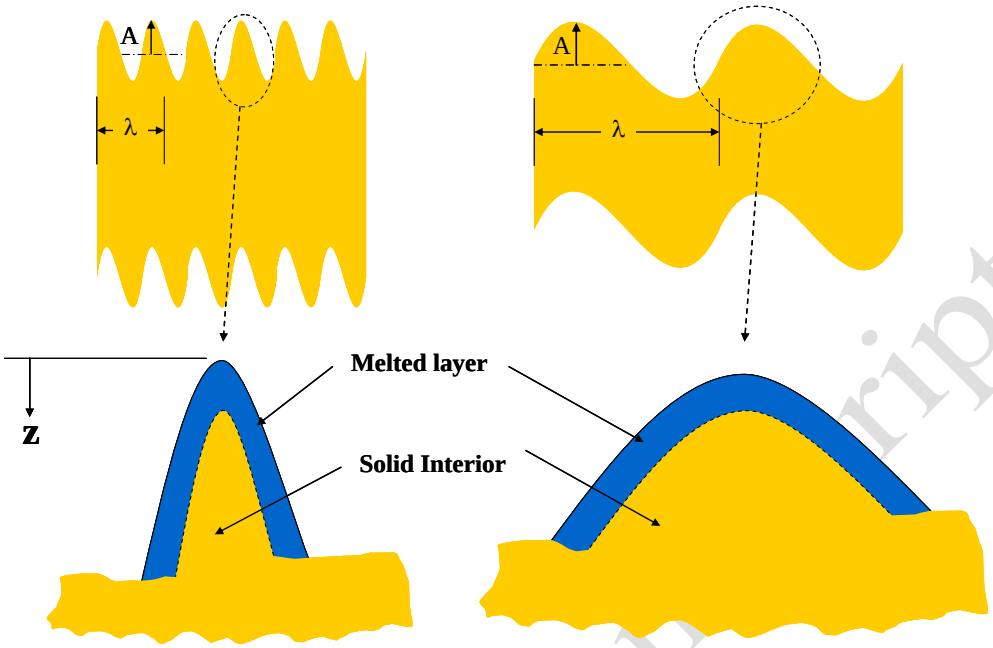

(a)

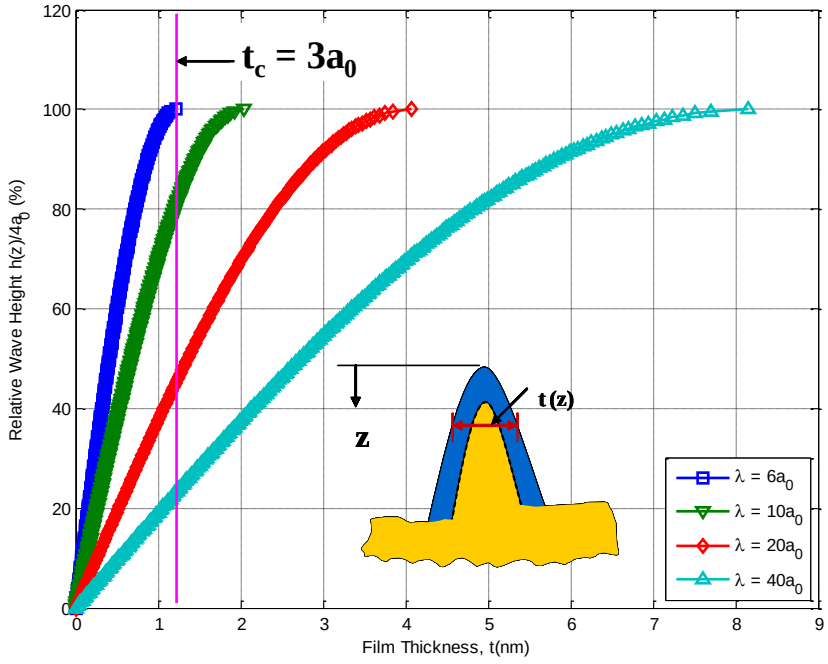

(b)

Figure 8: (a) Schematic showing relative coverage of the melted boundary layer with respect to the total area of the "sub-films", (b) plot showing change in "sub-film" thicknesses with respect to the change in vertical wave height measured from the peak of waves.